

# Interval Harmonic State Estimation of Three-phase Asymmetric Distribution Network by Integrating Multi-source Data

Lipeng Zhou, Zhenguo Shao, Guoyang Cheng, Junjie Lin, and Feixiong Chen, *Member, IEEE*

**Abstract**—Harmonic state estimation in distribution networks is essential for identifying harmonic sources. However, issues such as limited measurement redundancy, asynchronous measurements, and unbalanced load distributions in three-phase networks undermine the reliability of existing methods in practical applications. To address these issues, this paper proposes an interval harmonic state estimation method in three-phase unbalanced distribution networks, integrating data from multiple sources. First, the interval multi-source harmonic measurement dataset is constructed by integrating asynchronous harmonic measurement data from multiple sources. The time asynchrony of measurement data from power quality monitoring devices is calibrated using the sliding window weighted dynamic time warping algorithm. Second, the interval harmonic state estimation model for the three-phase asymmetric distribution network is constructed. The model is solved using the interval-weighted least squares method, enhanced by the improved Krawczyk operator, thereby minimizing the expansion resulting from interval operations. Finally, the feasibility and accuracy of the proposed interval harmonic state estimation method are validated.

**Index Terms**—Interval harmonic state estimation, three-phase distribution network, multi-source information, asynchronous measurements.

## I. INTRODUCTION

With the large number of distributed renewable energy sources and power electronic equipment connected to the grid, harmonics in the three-phase distribution networks have shown new characteristics,

including strong randomness, multiple sources, and strong coupling. These harmonics can induce system resonance, leading to equipment damage and protection device malfunction, thus affecting network stability and reliability [1], [2]. Therefore, it is necessary to identify the distribution of harmonic sources to regulate harmonics in distribution networks [3], [4]. Harmonic state estimation (HSE) is an effective technology used for monitoring and analyzing harmonics, providing a foundation for harmonic management and suppression [5], [6].

Unlike the symmetry observed in the three-phase parameters of transmission networks, three-phase distribution networks experience issues such as terminal phase loss and phase-to-phase mutual inductance [7]. The three phases in the distribution network are not transposed, leading to asymmetrical three-phase parameters along the line [8]. Furthermore, the three-phase distribution network accommodates concentrated and distributed loads along its lines. In certain areas, single-phase lines serve the loads, contributing to asymmetrical characteristics of the three-phase loads within the distribution network [9]. Moreover, the rising integration of distributed renewable energy, energy storage systems, and electric vehicles within distribution networks has intensified the asymmetrical characteristics of three-phase distribution systems [10], [11]. These factors make the simplified assumptions underlying traditional HSE methods unsuitable for distribution networks, thereby limiting their ability to accurately represent the system's actual operating state. Consequently, for three-phase asymmetry distribution networks, implementing three-phase HSE is essential for accurately describing and assessing the harmonic conditions of the network [12], [13]. However, two challenges arise when conducting HSE in three-phase asymmetric distribution networks.

The first challenge is the insufficient harmonic measurement devices in distribution networks [14]. Single-type harmonic measurement devices are sparsely deployed and do not provide coverage for all network nodes. This leads to unobservability in distribution networks [15], [16]. For unobservable networks, the differential synchronous phasor estimation is formulated

---

Received: March 20, 2025

Accepted: November 10, 2025

Published Online: March 1, 2026

Lipeng Zhou, Zhenguo Shao (corresponding author), Guoyang Cheng, Junjie Lin, and Feixiong Chen are with the College of Electrical Engineering and Automation, Fujian Smart Electrical Engineering Technology Research Center, Fuzhou University, Fuzhou 350108, China (e-mail: zlp197@126.com; shao.zg@fzu.edu.cn; cheng@fzu.edu.cn; linjunjie@fzu.edu.cn; feixiongchen@fzu.edu.cn).

DOI: 10.23919/PCMP.2024.000400

as an adaptive group sparse recovery problem by sparse technique [17]. In [18], a static HSE method based on a sparse Bayesian algorithm is proposed, assuming limited phasor measurement units (PMUs) are strategically placed along the feeder line. In [19], the sparse pattern based on physics is captured, and the harmonic estimation is carried out by using the mixed integer quadratic programming solver. In [20], the position of the harmonic source is identified by fitting harmonic current radiation and selecting the minimum fitting residual. In [21], the sparse Bayesian method estimates the harmonic state, with the least square method as the goal. In [22], independent component analysis estimates harmonics when unknown harmonic network parameters are considered. Although the above researches have achieved HSE with limited single-type measurement data, the accuracy of the results is dependent on the location and number of measurement points, and the essence of the low observability of the system has not changed. Therefore, the system's observability can be improved by integrating multiple sources of harmonic measurement data.

Nonetheless, the differing sampling characteristics of various harmonic measurement devices imply that the effectiveness of the multi-source fusion method will significantly impact the accuracy of the estimation results [23]. Multi-source measurement fusion methods focus on the fundamental wave domain [24]–[27]. In the realm of harmonics, the restricted variety of harmonic measurement devices has led to a lack of research on multi-source harmonic measurement fusion. In [28], two kinds of measurements, smart meter and transformer terminal units, are proposed to improve the system's observability, whereas in [29], transformer terminal units and power quality monitoring devices (PQMDs) measurements are applied to enhance system observability. A maximum entropy principle model is established for the harmonic current injected into the bus, enabling the calculation of its probability density function and facilitating optimal interpolation of harmonic data. In [30], a multi-source data-driven technique is proposed, which estimates the harmonic spectrum of substation feeder currents by leveraging data from PQMDs and the dispatching system. However, the above research defaults that the measurement data provided by PQMDs are definite values, ignoring the data's statistical characteristics. Concurrently, the incompatibility of multiple types of harmonic measurement data on the accuracy of HSE results is overlooked.

The second challenge is the heightened uncertainty of the system [31]. The intermittent nature of high-penetration distributed renewable energy, combined with the random charging patterns of large-scale electric vehicles, have amplified the volatility and

randomness within distribution networks [32], [33]. Numerous studies have examined the uncertainty in three-phase distribution networks, primarily focusing on the uncertainty of measurement data and power grid line parameters. The research methods can generally be classified into three categories: probability density function based, fuzzy membership function based, and interval arithmetic based [34]. Unlike the previous two methods, the interval method addresses uncertain variables without requiring extensive historical data to derive detailed probability density functions, which are difficult to obtain accurately. This approach only requires the upper and lower bounds of each variable, thereby avoiding additional human assumptions and minimizing the impact of subjective factors on the calculation results. In [35], the PQMD data is used to supplement PMU measurement data, and the line parameter estimation method of distribution network based on interval HSE is proposed. In [36], an interval least squares method considering parameter uncertainty is proposed, using sufficient PMU measurements to meet observability. However, most proposed interval HSE methods are primarily based on symmetry distribution networks. The idealized system environment makes it challenging to describe the actual harmonic characteristics accurately.

This paper proposes a multi-source data fusion method to estimate the interval harmonic state in three-phase asymmetric distribution networks. It considers the network characteristics, the limited number of harmonic measurement devices, and the asynchrony of different harmonic data. A multi-source harmonic measurement dataset is established by integrating harmonic data from multiple sources, and the interval method is used to represent harmonic uncertainty. Subsequently, an interval HSE model for the three-phase distribution network is established. The interval-weighted least squares method combined with the improved Krawczyk operator (KMWLS), is used to solve the problem. Finally, the validity of the proposed method is verified in the IEEE-34 and IEEE-123 systems. The main contribution is summarized as follows:

- 1) A multi-source asynchronous harmonic measurement data fusion strategy is proposed to address the unobservability of single-type harmonic measurements in three-phase distribution networks;
- 2) Novel algorithms are proposed to address harmonic measurement data asynchrony issues, including the sliding window weighted dynamic time warping algorithm and the artificial fish swarm algorithm with an adaptive memory mechanism;
- 3) An interval HSE method is proposed to address the uncertainty of the measurement data and network parameters, thereby enhancing the accuracy and reliability of the estimation results. Furthermore, this method

considers the three-phase asymmetric characteristics of distribution networks, which is more realistic than assuming symmetry.

The paper is structured as follows. Section II elaborates on the theoretical background of HSE and the modeling of the three-phase asymmetric distribution networks. Section III outlines the multi-source harmonic measurement fusion method, which solves the asynchronous problem between multi-source data. Section IV presents the improved solution method for three-phase interval HSE, and Section V discusses the simulation results that validate the preceding analysis. Finally, Section VI concludes the paper.

## II. HARMONIC STATE ESTIMATION OF DISTRIBUTION NETWORK

### A. Basic Theory

HSE is the process of solving the harmonic state of the entire network under the conditions of given topology, line parameters, and partial measurement sets. Its basic equation is:

$$\mathbf{z} = \mathbf{h}(x) + \boldsymbol{\varepsilon} \quad (1)$$

where  $\mathbf{z}$  is the quantity measurement;  $\boldsymbol{\varepsilon}$  is the measurement error;  $x$  is the state variable; and  $\mathbf{h}(\cdot)$  is the measurement function.

The optimal state variables are obtained using the weighted least squares (WLS) criterion, which minimizes the sum of weighted squares of measurement errors. The objective function can be expressed as:

$$\min J(x) = (\mathbf{z} - \mathbf{h}(x))^T \mathbf{R}^{-1} (\mathbf{z} - \mathbf{h}(x)) \quad (2)$$

where  $\mathbf{R}^{-1}$  is the weight of measurement  $\mathbf{z}$  and  $\mathbf{R} = \text{diag}[\sigma_1^2, \sigma_2^2, \dots, \sigma_m^2]$  ( $\sigma_i^2$  denotes the variance of the  $i$ th measurement error and  $i = 1, 2, \dots, m$ ); and  $J(x)$  is the objective function value. Optimal estimated states are solved by the Newton iteration method:

$$\partial J / \partial x = [\mathbf{H}(x)]^T \mathbf{R}^{-1} [\mathbf{z} - \mathbf{h}(x)] = 0 \quad (3)$$

$$[\mathbf{H}(x)]^T \mathbf{R}^{-1} \mathbf{H}(x) \Delta x = [\mathbf{H}(x)]^T \mathbf{R}^{-1} [\mathbf{z} - \mathbf{h}(x)] \quad (4)$$

where  $\mathbf{H}(\cdot)$  is the Jacobian matrix of the measurement function and  $\mathbf{H}(x) = \partial \mathbf{h}(x) / \partial x$ .

### B. Establish the Three-phase Asymmetric Distribution Network Model

The distribution network topology and operating conditions are complicated and changeable, with significant operational uncertainty, asymmetric three-phase loads, and a growing impedance ratio. Therefore, this paper adopts the three-phase three-wire system with an ungrounded neutral point and establishes the three-phase three-wire model of the distribution network with a standard  $\pi$ -type equivalent circuit, as shown in Fig. 1.

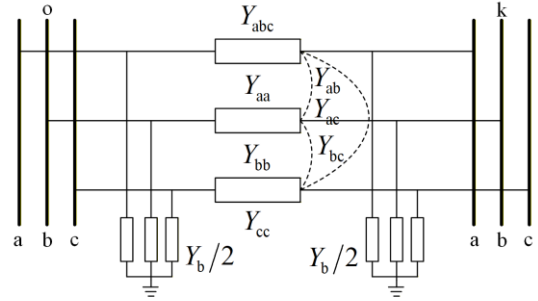


Fig. 1.  $\pi$  type equivalent circuit topology.

To facilitate the extraction of the line admittance matrix, the matrix index and matrix paradigm transformation technology are introduced into the construction of the admittance matrix. This approach enables normative mapping from the equipment sequence parameter list of the single-phase power grid to the admittance matrix elements of the three-phase power grid. It also improves the efficiency of randomly accessing the three-phase admittance matrix. Take the line admittance  $\mathbf{Y}_{ok} = \mathbf{Y}_{l,ok} + j\mathbf{Y}_{b,ok}$  as an example:

$$\left\{ \begin{array}{l} \mathbf{Y}_{l,ok} = \begin{bmatrix} \mathbf{Y}_{l,ok}^{aa} & \mathbf{Y}_{l,ok}^{ab} & \mathbf{Y}_{l,ok}^{ac} \\ \mathbf{Y}_{l,ok}^{ba} & \mathbf{Y}_{l,ok}^{bb} & \mathbf{Y}_{l,ok}^{bc} \\ \mathbf{Y}_{l,ok}^{ca} & \mathbf{Y}_{l,ok}^{cb} & \mathbf{Y}_{l,ok}^{cc} \end{bmatrix} \\ \mathbf{Y}_{b,ok} = \begin{bmatrix} \mathbf{Y}_{b,ok}^{aa} & \mathbf{Y}_{b,ok}^{ab} & \mathbf{Y}_{b,ok}^{ac} \\ \mathbf{Y}_{b,ok}^{ba} & \mathbf{Y}_{b,ok}^{bb} & \mathbf{Y}_{b,ok}^{bc} \\ \mathbf{Y}_{b,ok}^{ca} & \mathbf{Y}_{b,ok}^{cb} & \mathbf{Y}_{b,ok}^{cc} \end{bmatrix} \end{array} \right. \quad (5)$$

$$\left\{ \begin{array}{l} \mathbf{C}_{l,o} = f_{\text{sparse}}(\mathbf{C}_o, 1:1:n_{\text{line}}, \mathbf{E}_{n_{\text{line}}}) \otimes \mathbf{I}_3 \\ \mathbf{C}_{l,k} = f_{\text{sparse}}(\mathbf{C}_k, 1:1:n_{\text{line}}, \mathbf{E}_{n_{\text{line}}}) \otimes \mathbf{I}_3 \end{array} \right. \quad (6)$$

where  $f_{\text{sparse}}$  is the sparse matrix construction function;  $\mathbf{C}_o$  and  $\mathbf{C}_k$  represent the index numbers of nodes  $o$  and  $k$  respectively;  $n_{\text{line}}$  is the number of network branches;  $\mathbf{E}_{n_{\text{line}}}$  is a dimensional column vector  $n_{\text{line}}$  with all elements being 1;  $\otimes$  represents the Kronecker product; and  $\mathbf{I}_3$  is the identity matrix. Arranged by line numbers, the three-phase line admittance series submatrix  $\mathbf{Y}_{l,ok}^{abc}$  can be obtained. Perform matrix paradigm transformation on the submatrix  $\mathbf{Y}_l^{abc}$ , and obtain the series impedance part  $\mathbf{Y}_l$  of the node three-phase admittance matrix:

$$\mathbf{Y}_l^{abc} = [\mathbf{Y}_{l,ok(1)}^{abc} \quad \dots \quad \mathbf{Y}_{l,ok(m)}^{abc} \quad \dots \quad \mathbf{Y}_{l,ok(n_{\text{line}})}^{abc}]^T \quad (7)$$

$$\mathbf{Y}_l = \mathbf{C}_{l,o} f_{\text{diag}}(\mathbf{Y}_l^{abc}) \mathbf{C}_{l,o}^T + \mathbf{C}_{l,k} f_{\text{diag}}(\mathbf{Y}_l^{abc}) \mathbf{C}_{l,k}^T + \mathbf{C}_{l,o} f_{\text{diag}}(-\mathbf{Y}_l^{abc}) \mathbf{C}_{l,k}^T + \mathbf{C}_{l,k} f_{\text{diag}}(-\mathbf{Y}_l^{abc}) \mathbf{C}_{l,o}^T \quad (8)$$

where  $\mathbf{Y}_{l,ik(m)}^{abc}$  is the admittance matrix with line number  $m$  and  $f_{\text{diag}}(\cdot)$  is the block diagonal function for the corresponding matrix; and  $\mathbf{Y}_B$  is constructed in the

same way. To estimate the harmonic state, it is sufficient to substitute the fundamental parameters in the admittance matrix with harmonic parameters.

The presence of asymmetric loads and line parameters in the three-phase distribution network causes some buses and branches to be out of phase. A virtual branch is introduced to the missing phase to prevent the three-phase impedance matrix and the state estimation information matrix from becoming non-invertible due to singular matrices. For example, for the two-phase line o–k lacking phase A, the three-phase admittance matrix after introducing the virtual branch is as follows:

$$\left\{ \begin{array}{l} \mathbf{Y}_k = \begin{bmatrix} y_k^{aa} & 0 & 0 \\ 0 & y_k^{bb} & y_k^{bc} \\ 0 & y_k^{cb} & y_k^{cc} \end{bmatrix} \\ \mathbf{Y}_{o,k} = \begin{bmatrix} y_{o,k}^{aa} & 0 & 0 \\ 0 & y_{o,k}^{bb} & y_{o,k}^{bc} \\ 0 & y_{o,k}^{cb} & y_{o,k}^{cc} \end{bmatrix} \end{array} \right. \quad (9)$$

However, the positive value of the main diagonal element of phase A will introduce errors in the estimation, which will affect the HSE accuracy. Therefore, the branch of phase A can be regarded as an open circuit, with the measurement data of the missing phase set to 0 accordingly. Then, the calculation formulas for branch current and bus current are as follows:

$$\left\{ \begin{array}{l} \mathbf{I}_{o,k} = [I_{o,k}^a, I_{o,k}^b, I_{o,k}^c]^T = \mathbf{Y}_{o,k}(\mathbf{U}_o - \mathbf{U}_k) + \mathbf{I}_{o(g)} = \\ \quad \mathbf{Y}_{o,k}(\mathbf{U}_o - \mathbf{U}_k) + \mathbf{Y}_o \mathbf{U}_o / 2 \\ \mathbf{I}_o = [I_o^a, I_o^b, I_o^c]^T = \mathbf{Y}_o \mathbf{U}_o \\ \mathbf{U}_o = [U_o^a, U_o^b, U_o^c]^T \end{array} \right. \quad (10)$$

The calculation formulas of the YnD-type transformer branch current are as follows:

$$\begin{bmatrix} \mathbf{I}_{ps} \\ \mathbf{I}_{sp} \end{bmatrix} = \begin{bmatrix} \mathbf{Y}_{pp}^{\{a,b,c\}} & \mathbf{Y}_{ps}^{\{a,b,c\}} \\ \mathbf{Y}_{sp}^{\{a,b,c\}} & \mathbf{Y}_{ss}^{\{a,b,c\}} \end{bmatrix} \times \begin{bmatrix} \mathbf{U}_p \\ \mathbf{U}_s \end{bmatrix} \quad (11)$$

$$\left\{ \begin{array}{l} \mathbf{Y}_{pp} = \mathbf{Y}_I \\ \mathbf{Y}_{ss} = \mathbf{Y}_{II} \\ \mathbf{Y}_{ps} = \mathbf{Y}_{III} \\ \mathbf{Y}_{sp} = \mathbf{Y}_{III}^T \end{array} \right. \quad (12)$$

$$\left\{ \begin{array}{l} \mathbf{Y}_I = y_t \begin{bmatrix} 1 & 0 & 0 \\ 0 & 1 & 0 \\ 0 & 0 & 1 \end{bmatrix} \\ \mathbf{Y}_{II} = \frac{y_t}{3} \begin{bmatrix} 2 & -1 & -1 \\ -1 & 2 & -1 \\ -1 & -1 & 2 \end{bmatrix} \\ \mathbf{Y}_{III} = \frac{y_t}{\sqrt{3}} \begin{bmatrix} -1 & 1 & 0 \\ 0 & -1 & -1 \\ 1 & 0 & -1 \end{bmatrix} \end{array} \right. \quad (13)$$

where  $I_{ps}$  and  $I_{sp}$  are the branch current;  $U_p$  is the node voltage of bus p;  $U_s$  is the node voltage of bus s; and  $y_t$  is the per unity transformer leakage admittance.

### III. MULTI-SOURCE ASYNCHRONOUS HARMONIC MEASUREMENT DATA FUSION

#### A. The Harmonic Measurement Devices in Distribution Networks

Currently,  $\mu$ PMU and PQMD are the primary sources of harmonic data in three-phase distribution networks. The specific characteristics of their harmonic measurement data are detailed in Table I.

TABLE I  
HARMONIC MEASUREMENT DEVICE CHARACTERISTICS

Measurement device	$\mu$ PMU	PQMD
Refresh rates	20 ms	1–3 min
Data components	Node voltage and current vectors, branch power, node injection power	Node voltage amplitude, node current amplitude, harmonic phase angle based on local A phase voltage phase angle, node injected active and reactive power
Time scale	Exist	Absent
Transmission delays	Low	Medium
Data accuracy	$\pm 0.05$	$\pm 2$

The  $\mu$ PMU is primarily installed at substations and other critical buses. Although it can provide synchronized phasor data in real time, there may be delays in processing and analyzing harmonic components due to limitations in the device's computational capacity and data transmission bandwidth. The  $\mu$ PMU mainly focuses on low-order harmonics in the power grid. Additionally, several characteristics of PQMD measurement data are worth noting: 1) PQMD records the maximum, minimum, average, and 95% probability maximum of harmonic measurements during the detection period, thus, PQMD measurement data is statistical data or is interval data; 2) PQMD lacks time correspondence between multiple monitoring devices, with less precise time synchronization than  $\mu$ PMU; and 3) PQMD stores harmonic phase angle based on the local fundamental voltage phase angle of phase A, instead of the actual phase angle.

Since PQMD and  $\mu$ PMU belong to different technical platforms, there are numerous differences in their harmonic measurement data: 1) different data refresh rates; 2) different data transmission delays; and 3) different data components. Integrating PQMD and  $\mu$ PMU measurements directly may cause data compatibility issues, resulting in discrepancies between the constructed mathematical model and the actual system.

This can compromise the accuracy of HSE results, potentially misleading operational and maintenance decisions, affecting the identification of harmonic sources, and jeopardizing the stability and security of the system. Therefore, this paper considers these differences when fusing multi-source harmonic measurement data and subsequently proposes a multi-source harmonic measurement data fusion framework.

### B. Construct a Data Fusion Framework for Integrating Multi-source Harmonic Measurements

Among the differences between PQMD and  $\mu$ PMU data, data refresh rates and transmission delays fall under the time synchronization issues category. For multi-source harmonic measurements to be used effectively for HSE at a given moment, its time synchronization must meet specific requirements. Thus, to enhance observability and reduce the asynchrony error of harmonic measurement data in the three-phase distribution network, this paper focuses on integrating multi-source harmonic data in terms of data time scale and data refresh rates, establishing a multi-scale harmonic measurement data fusion framework, as shown in Fig. 2.

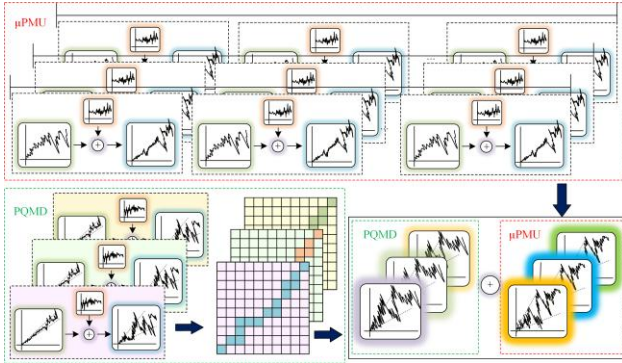


Fig. 2. Diagram of multi-source harmonic measurement fusion.

The specific fusion steps are as follows.

1) A sliding window weighted dynamic time warping (SWWDTW) algorithm is proposed to solve the problem of time asynchronism among PQMD measurement points. The PQMD dataset is constructed by calculating the time distance between the sampled data of each PQMD monitoring device within the time window, and selecting the minimum time distance of the harmonic measurement data from each PQMD measurement point. This part of the research corresponds to Section III.C.

2) The artificial fish swarm algorithm based on the adaptive memory mechanism (AMAFSA) is adopted to calculate fundamental wave phase information. Then, combined with phase information recorded in PQMD, the harmonic phase information calibration is realized. This part of the research corresponds to Section III.D.

3) Using the information domain buffer technology, the adjacent measurement time of the reference PQMD is used as the buffer time length of  $\mu$ PMU measurement,

and then interval  $\mu$ PMU measurements are obtained. An interval multi-source harmonic measurement data set is constructed. This part of the research corresponds to Section III.E.

### C. Select the Measurement Data with Minimum Asynchronous Time of PQMD Measurement Data

To minimize the asynchronous time of PQMD data in the measurement data set, this paper proposes a SWWDTW algorithm. Assume there are  $n$  sampling sequences in a PQMD measurement data, and  $N$  measurement points constitute the PQMD dataset  $X = \{X_i\}_{i=1}^N$ . For the PQMD series  $X_i = (x_{i1}, \dots, x_{it}, \dots, x_{in})$  and  $X_j = (x_{j1}, \dots, x_{jt'}, \dots, x_{jn})$ , to avoid the unnatural warping caused by traditional dynamic time warping algorithm during matching [37], the sliding window technology is used, which generates a window timing matrix by moving a window with a given time window width  $T$ . The series  $X_i$  and  $X_j$  are represented as  $X_{i-T\text{-window}} = (x_{i,k}, \dots, x_{i,k+T})$  and  $X_{j-T\text{-window}} = (x_{j,k}, \dots, x_{j,k+T})$ . Considering that PQMD is only installed at key buses of the distribution network, a weight vector  $w_i = (w_{i1}, w_{i2}, \dots, w_{iN})$  is assigned to each PQMD measuring point, defined as:

$$w_{it} = \frac{\sum_{x_j} \frac{1}{|W_{ij}^t|} \left( \sum_{(t,t') \in W_{ij}^t} (x_{it} - x_{it'})^2 \right)}{\tau + \sum_{x_j} \frac{1}{|W_{ij}^t|} \left( \sum_{(t,t') \in W_{ij}^t} (x_{it} - x_{jt'})^2 \right)} \quad (14)$$

where  $W_{ij}^t$  is the alignment path between the sequences  $X_i$  and  $X_j$ ; in addition, a minimum value  $\tau$  is added to the denominator, with a value of  $10^{-6}$ , to prevent the denominator from being zero.

Then, the distance between any two points in the two sequences becomes:

$$d(x_{it}, x_{jt'}) = \sqrt{\sum_{t=1}^m (w_{it} x_{it} - w_{jt'} x_{jt'})^2} \quad (15)$$

By assigning different weights to each data series, the asynchrony of each measurement data can be better distinguished. Subsequently, the cumulative distance matrix  $D$  between two series within the time window can be constructed, and the cumulative distance matrix at any time can be expressed as:

$$D(x_{it}, x_{jt'}) = d(x_{it}, x_{jt'}) + \min \{ D(x_{i,t-1}, x_{jt'}), D(x_{it}, x_{j,t-1}), D(x_{i,t-1}, x_{j,t-1}) \} \quad (16)$$

Then, based on dynamic programming principles and related constraints, the path with the smallest cumulative distance matrix  $D$  matches the two sequences. The alignment path  $W_{ij}$  and the constraints are expressed as:

$$W_{ij} = ((x_{i1}, x_{j1}), \dots, (x_{it}, x_{jt}), \dots, (x_{in}, x_{jn})) \quad (17)$$

$$\begin{cases} W_{x_i}(1) = W_{x_j}(1) = 1 \\ W_{x_i}(t) = W_{x_j}(t) = n \\ W_{x_i}(t+1) \geq W_{x_j}(t) \\ W_{x_j}(t+1) \geq W_{x_j}(t) \\ W_{x_i}(t+1) - W_{x_j}(t) \leq 1 \end{cases} \quad (18)$$

Finally, the minimum time distance sequence set  $W = \{W_{ij}\}_{j=1}^N$  between the sampled data of PQMD measurement points and the benchmark PQMD measurement point can be obtained.

#### D. Calibration Interval Harmonic Phase Angle Based on Adaptive Memory Mechanism for Artificial Fish Swarm

To ensure the correctness and accuracy of HSE results, the AMAFSA method estimates the fundamental wave state. Subsequently, the missing fundamental phase angle information for the harmonic monitoring points is calculated.

The AFSA is a heuristic algorithm with global optimization capabilities and low sensitivity to initial values. Its specific formula can be found in [38]. However, the hyperparameter settings of AFSA usually rely on manual experience, which may not ensure optimal convergence accuracy. Therefore, this paper introduces a parameter adaptive adjustment mechanism to set the values of the field of view  $v$  and step size  $s$  at different times to avoid falling into local optima:

$$v = v_{\min} + (v_{\max} - v_{\min}) \times (1 - f(x_{\text{gbest}}) / f(x_i)) \quad (19)$$

$$s = s_{\min} + (s_{\max} - s_{\min}) \times (1 - f(x_{\text{gbest}}) / f(x_i)) \quad (20)$$

where  $f(x_i)$  is the fitness value of the position;  $f(x_{\text{gbest}})$  is the current global optimal value;  $v_{\min}$  is the lower bound of the artificial fish visual field, with a value of 0.1;  $v_{\max}$  is the upper bound of the artificial fish field of view, with a value of 0.9;  $s_{\min}$  is the lower bound of the artificial fish step size, with a value of 0.1; and  $s_{\max}$  is the upper bound of the artificial fish step size, with a value of 0.9.

Concurrently, the memory mechanism is introduced to help the artificial fish compare its fitness value with its optimal position while seeking the optimal value. The expression of memory behavior is:

$$x_i^{\text{best}}(t) = \begin{cases} x_i(t), & \text{if } f_i(t) < f_i^{\text{best}}(t-1) \\ x_i^{\text{best}}(t-1), & \text{otherwise} \end{cases} \quad (21)$$

$$f_i^{\text{best}}(t) = \min(f_i(t), f_i^{\text{best}}(t-1)) \quad (22)$$

Finally, the AMAFSA method sets the state quantity

as the fundamental voltage amplitude and phase angle. The fitness objective function is formed:

$$f = \min_x \left\{ \frac{1}{2} w \|z - Hx\|_2^2 + \lambda \|x\|_1 \right\} \quad (23)$$

where  $w$  is the measurement weight;  $H$  is the state function; and  $\lambda \in [0, 1]$  is the penalty factor. This paper determines the value with 0.05. The AMAFSA is set with the following parameters: population size of 68, maximum number of iterations of 10, initial step size of 0.5, initial visual range of 0.3, and crowding factor of 0.5.

According to the recorded phase information of PQMD and the calculated fundamental wave phase information, the harmonic phase angle of the harmonic monitoring point  $\{[z_{\text{PQMD}, \theta}^h]\}$  is calibrated:

$$[\theta_i^h] = [\phi_i^h] + [\theta_i^l] \quad (24)$$

where  $[\theta_i^h]$  is the interval harmonic phase angle;  $[\phi_i^h]$  is the recorded interval harmonic phase information of PQMD; and  $[\theta_i^l]$  is the calculated fundamental wave phase information.

#### E. Create a Multi-source Harmonic Measurement Set

This paper establishes a multi-source harmonic measurement dataset to achieve HSE by integrating  $\mu$ PMU and PQMD data. The multi-source data fusion framework for HSE is shown in the Fig. 3.

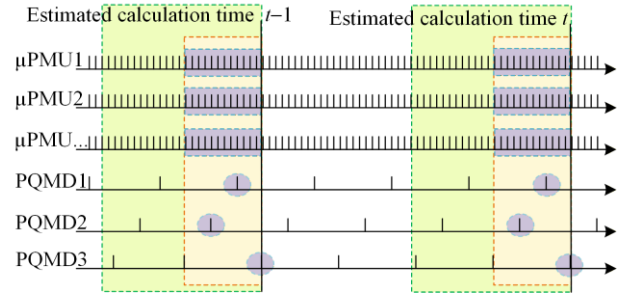


Fig. 3. Schematic diagram of multi-source measurement data fusion in distribution network.

The specific approach is as follows.

First, the minimum and maximum values of harmonic and fundamental statistics are extracted from each PQMD measurement  $W = \{W_{ij}\}_{j=1}^N$  to construct an interval measurement dataset of PQMD:

$$\{[z_{\text{PQMD}}^h]\} = \{[I_i^h], [U_i^h]\} \quad (25)$$

where  $\{[z_{\text{PQMD}}^h]\}$  is the PQMD interval harmonic measurement data set;  $|I_i^h|$  and  $|U_i^h|$  are the amplitude measurement data of the PQMD interval node harmonic current and node harmonic voltage, respectively.

Then, the interval between the two sampled data of the benchmark PQMD is used as the  $\mu$ PMU buffer, with the assumption that the buffer has cached many  $\mu$ PMU sampled data. After converting the  $\mu$ PMU amplitude and phase angle data into a rectangular coordinate system, the maximum and minimum values of the real and imaginary parts are extracted to establish an interval  $\mu$ PMU phase measurement set:

$$\left\{ \begin{aligned} \left[ \mathbf{z}_{\mu\text{PMU}}^h \right] &= \left[ \underline{z}_{\mu\text{PMU}}^{h,\text{re}}, \bar{z}_{\mu\text{PMU}}^{h,\text{re}} \right] + j \left[ \underline{z}_{\mu\text{PMU}}^{h,\text{im}}, \bar{z}_{\mu\text{PMU}}^{h,\text{im}} \right] \\ \underline{z}_{\mu\text{PMU}}^h &= \min \left\{ z_{\mu\text{PMU},1}^h, \dots, z_{\mu\text{PMU},p}^h \right\} \\ \bar{z}_{\mu\text{PMU}}^h &= \max \left\{ z_{\mu\text{PMU},1}^h, \dots, z_{\mu\text{PMU},p}^h \right\} \\ \left[ \dot{\mathbf{U}}_{\mu\text{PMU},i}^h \right] &= \left[ \underline{e}_{\mu\text{PMU},i}^h, \bar{e}_{\mu\text{PMU},i}^h \right] + j \left[ \underline{f}_{\mu\text{PMU},i}^h, \bar{f}_{\mu\text{PMU},i}^h \right] \\ \left[ \dot{\mathbf{I}}_{\mu\text{PMU},ij}^h \right] &= \left[ \underline{I}_{\mu\text{PMU},ij}^{h,\text{re}}, \bar{I}_{\mu\text{PMU},ij}^{h,\text{re}} \right] + j \left[ \underline{I}_{\mu\text{PMU},ij}^{h,\text{im}}, \bar{I}_{\mu\text{PMU},ij}^{h,\text{im}} \right] \end{aligned} \right. \quad (26)$$

where  $\left\{ \left[ \mathbf{z}_{\mu\text{PMU}}^h \right] \right\}$  is the  $\mu$ PMU interval harmonic measurement data set;  $\underline{z}_{\mu\text{PMU}}^h$  and  $\bar{z}_{\mu\text{PMU}}^h$  are the minimum and maximum values of the real or imaginary part of the  $\mu$ PMU harmonic measurement data in the buffer period, respectively;  $\underline{I}_{\mu\text{PMU},ij}^{h,\text{re}}$  and  $\underline{I}_{\mu\text{PMU},ij}^{h,\text{im}}$  are the minimum values of the real and imaginary parts of the branch harmonic current, respectively; while  $\bar{I}_{\mu\text{PMU},ij}^{h,\text{re}}$  and  $\bar{I}_{\mu\text{PMU},ij}^{h,\text{im}}$  are the maximum values of the real and imaginary parts of the branch harmonic current, respectively.

Finally, the harmonic interval measurement data set  $\left[ \mathbf{z}^h \right]$  is constructed as:

$$\left\{ \left[ \mathbf{z}^h \right] \right\} = \left\{ \left[ \mathbf{z}_{\mu\text{PMU}}^h \right], \left[ \mathbf{z}_{\text{PQMD}}^h \right], \left[ \mathbf{z}_{\text{PQMD},\theta}^h \right] \right\} \quad (27)$$

#### IV. INTERVAL HARMONIC STATE ESTIMATION OF THREE-PHASE ASYMMETRIC DISTRIBUTION NETWORK BY INTEGRATING MULTI-SOURCE DATA

##### A. Interval Harmonic State Estimation of Three-phase Asymmetric Distribution Network

For the three-phase asymmetrical distribution network, three-phase HSE is required to describe the network's harmonic conditions accurately. Some measurement devices (such as PQMDs) provide statistical data in practical three-phase asymmetrical distribution networks. Additionally, while the actual values of network parameters are difficult to obtain, their upper and lower bounds can usually be determined. Therefore, this paper proposes a three-phase asymmetric interval HSE model using interval numbers. The interval HSE model is as follows:

$$\left[ \mathbf{H} \right]^T \mathbf{W} \left[ \mathbf{H} \right] \left[ \mathbf{x} \right] := \left[ \mathbf{H} \right]^T \mathbf{W} \left[ \mathbf{z} \right] \quad (28)$$

$$\left\{ \begin{aligned} \left[ \mathbf{z} \right] &= \begin{bmatrix} \left[ \mathbf{V}_{i,\text{equ}}^{h,\varphi} \right] \\ \left[ \mathbf{V}_{i,\text{mea}}^{h,\varphi} \right] \\ \left[ \mathbf{I}_{ik,\text{equ}}^{h,\varphi} \right] \\ \left[ \mathbf{I}_{ik,\text{mea}}^{h,\varphi} \right] \end{bmatrix} = \begin{bmatrix} \left[ \mathbf{z}_i^\varphi \right] \\ \vdots \\ \left[ \mathbf{z}_m^\varphi \right] \end{bmatrix} \\ \left[ \mathbf{H} \right] &= \begin{bmatrix} \left[ \mathbf{Y}_{i,h}^{-1} \right] \\ \left[ \mathbf{Y}_{i,h}^{-1} \right] \\ \left[ \mathbf{Y}_{ik}^h \right] \\ \left[ \mathbf{Y}_{ik}^h \right] \end{bmatrix} = \begin{bmatrix} \left[ \mathbf{H}_{1,1} \right] & \cdots & \left[ \mathbf{H}_{1,n} \right] \\ \vdots & & \vdots \\ \left[ \mathbf{H}_{m,1} \right] & \cdots & \left[ \mathbf{H}_{m,n} \right] \end{bmatrix} \end{aligned} \right. \quad (29)$$

$$\left\{ \begin{aligned} \left[ \mathbf{x} \right] &= \left[ \mathbf{I}_i^{h,\varphi} \right] = \left\{ \mathbf{x} \in R^{n \times 1} : \mathbf{H}\mathbf{x} \in \left[ \mathbf{z} \right]; \varphi = \text{A,B,C} \right\} \\ \left[ \mathbf{z} \right] &= \left\{ \begin{aligned} \mathbf{z} \in R^{m \times 1} : \underline{z}_j^\varphi \leq z_j^\varphi \leq \bar{z}_j^\varphi; k = 1, 2, \dots, m; \\ \varphi = \text{A,B,C} \end{aligned} \right\} \\ \left[ \mathbf{H} \right] &= \left\{ \begin{aligned} \mathbf{H} \in R^{(m \times n)} : \underline{H}_{i,k} \leq H_{i,k} \leq \bar{H}_{i,k}; i = 1, 2, \dots, n; \\ k = 1, 2, \dots, m; H_{i,k} \in R^{(\varphi \times \varphi)}; \varphi = \text{A,B,C} \end{aligned} \right\} \end{aligned} \right. \quad (30)$$

where  $\left[ \mathbf{x} \right]$  is the inject current state variables for interval nodes;  $\left[ \mathbf{z} \right]$  is the measured value of interval node voltage and branch current; and  $\left[ \mathbf{H} \right]$  is the select the Jacobian matrix of interval measurement function corresponding to the measured value. By introducing the transition interval vector  $\left[ \mathbf{y} \right]$ , the formula can be further equivalently transformed into:

$$\begin{bmatrix} \left[ \mathbf{H} \right] & -\mathbf{I} \\ 0 & \left[ \mathbf{H} \right]^T \mathbf{W} \end{bmatrix} \times \begin{bmatrix} \left[ \mathbf{x} \right] \\ \left[ \mathbf{y} \right] \end{bmatrix} = \begin{bmatrix} \left[ \mathbf{z} \right] \\ 0 \end{bmatrix} \quad (31)$$

It can be simplified as:

$$\left[ \mathbf{A} \right] \left[ \mathbf{X} \right] = \left[ \mathbf{b} \right] \quad (32)$$

$$\left\{ \begin{aligned} \left[ \mathbf{A} \right] &= \begin{bmatrix} \left[ \mathbf{H} \right] & -\mathbf{I} \\ 0 & \left[ \mathbf{H} \right]^T \mathbf{W} \end{bmatrix} \\ \left[ \mathbf{X} \right] &= \begin{bmatrix} \left[ \mathbf{x} \right] \\ \left[ \mathbf{y} \right] \end{bmatrix} \\ \left[ \mathbf{b} \right] &= \begin{bmatrix} \left[ \mathbf{z} \right] \\ 0 \end{bmatrix} \end{aligned} \right. \quad (33)$$

The interval analysis method is widely used for solving interval linear equations, and this paper uses an improved Krawczyk operator to solve interval linear equation systems. The specific process is as follows: Assuming that  $\left[ \mathbf{A} \right]$  and  $\left[ \mathbf{b} \right]$  are both non-singular interval matrices, for  $\forall \mathbf{A} \in \left[ \mathbf{A} \right], \forall \mathbf{b} \in \left[ \mathbf{b} \right]$ , and any given

non-singular deterministic matrix  $\mathbf{C}$ , there is the following relationship:

$$\mathbf{A}^{-1}\mathbf{b} = \mathbf{C}\mathbf{b} - (\mathbf{C}\mathbf{A} - \mathbf{I})\mathbf{A}^{-1}\mathbf{b} \in \mathbf{C}[\mathbf{b}] - (\mathbf{C}[\mathbf{A}] - \mathbf{I})[\mathbf{X}] \quad (34)$$

The iterative equation is defined as follows:

$$[\mathbf{X}^{k+1}] = (\mathbf{C}[\mathbf{b}] - (\mathbf{C}[\mathbf{A}] - \mathbf{I})[\mathbf{X}^k]) \cap [\mathbf{X}^k] \quad (35)$$

The Moore form of the Krawczyk operator is adopted in this paper. That is,  $\mathbf{C}$  is taken as the inverse matrix form of  $\mathbf{A}^m$  as follows:

$$\mathbf{C} = (\mathbf{A}^m)^{-1} \quad (36)$$

$$\mathbf{A}^m = \text{Mid}([\mathbf{A}]) = \begin{bmatrix} \text{Mid}([a_{11}]) & \text{Mid}([a_{12}]) & \cdots & \text{Mid}([a_{1n}]) \\ \text{Mid}([a_{21}]) & \text{Mid}([a_{22}]) & \cdots & \text{Mid}([a_{2n}]) \\ \vdots & \vdots & & \vdots \\ \text{Mid}([a_{m1}]) & \text{Mid}([a_{m2}]) & \cdots & \text{Mid}([a_{mn}]) \end{bmatrix} \quad (37)$$

where  $\text{Mid}(\cdot)$  is the median function of the interval number.

When the magnitude of the infinite norm of the interval solution vector meets the given convergence criterion, the iteration is stopped:

$$\left\| \text{Wid}([\mathbf{x}^k]) \right\|_{\infty} - \left\| \text{Wid}([\mathbf{x}^{k+1}]) \right\|_{\infty} < \varepsilon \quad (38)$$

where  $\left\| \text{Wid}([\mathbf{x}^k]) \right\|_{\infty}$  is the interval width function;  $\|\cdot\|_{\infty}$  denotes the infinity norm, which typically represents the maximum absolute value of a vector's components; and the convergence criterion  $\varepsilon$  is a given positive number approaching 0, normally set to  $10^{-6}$ .

However, the traditional Krawczyk operator generally employs the solution derived from the interval Gaussian elimination (IGE) method as the initial value. The IGE method is affected by the correlation of uncertain variables, which results in overly conservative solutions that diminish their practical reference value. To avoid over-expansion of the final solution, this paper adopts the improved initial solution; the specific process is as follows.

From  $\mathbf{A}\hat{\mathbf{X}} = \mathbf{b}$ , the estimated value  $\hat{\mathbf{X}}$  can be obtained as:

$$\hat{\mathbf{X}} = \mathbf{C}\mathbf{b} + (\mathbf{I} - \mathbf{C}\mathbf{A})\hat{\mathbf{X}} \quad (39)$$

Further calculations show that:

$$\left\| \hat{\mathbf{X}} \right\| \leq \left\| \mathbf{C}\mathbf{b} \right\| + \left\| \mathbf{I} - \mathbf{C}\mathbf{A} \right\| \times \left\| \hat{\mathbf{X}} \right\| \quad (40)$$

After extracting the common factor, the formula is:

$$(1 - \varpi) \left\| \hat{\mathbf{X}} \right\| \leq \left\| \mathbf{C}\mathbf{b} \right\| \quad (41)$$

where  $\varpi = \left\| \mathbf{I} - \mathbf{C}\mathbf{A} \right\|_{\infty} < 1$  exists for  $\mathbf{C}$ , which is the inverse of the  $\text{Mid}([\mathbf{A}])$ . In addition, due to  $\left\| \mathbf{I} - \mathbf{C}\mathbf{A} \right\|_{\infty} \leq \left\| \mathbf{I} - \mathbf{C}\mathbf{A} \right\|_{\infty}$ , the initial solution is as follows:

$$[\mathbf{X}]^{(0)} = \left[ \frac{\left\| \mathbf{C}\mathbf{b} \right\|_{\infty}}{\varpi - 1}, \frac{\left\| \mathbf{C}\mathbf{b} \right\|_{\infty}}{1 - \varpi} \right]^T \quad (42)$$

## B. Evaluation Indicators

To verify the accuracy, completeness, and conservatism of the interval HSE results, considering the uncertainty of the distribution network, this paper introduces several evaluation indicators. These include the upper bound root mean square of the interval estimation  $\mathfrak{g}$ , the average completeness index  $\zeta$ , and the average conservatism index  $\xi$ .

$$\mathfrak{g} = \sqrt{\left( \frac{1}{N} \sum_{k=1}^N (\mathbf{x}_{k,\text{up}}^h - [\hat{\mathbf{x}}_{k,\text{up}}^h])^T (\mathbf{x}_{k,\text{up}}^h - [\hat{\mathbf{x}}_{k,\text{up}}^h]) \right)} \quad (43)$$

$$\zeta = \frac{1}{N} \sum_{k=1}^N \kappa_k, \quad \kappa_k = \begin{cases} 1, & \text{if } x_i^h \in [\hat{x}_i^h] \\ 0, & \text{if } x_i^h \notin [\hat{x}_i^h] \end{cases} \quad (44)$$

$$\xi = \frac{1}{N} \sum_{k=1}^N \left| \frac{\hat{\mathbf{x}}_{k,\text{up}}^h - \hat{\mathbf{x}}_{k,\text{down}}^h}{\mathbf{x}_{k,\text{up}}^h - \mathbf{x}_{k,\text{down}}^h} \right| \quad (45)$$

where  $[\hat{\mathbf{x}}_{k,\text{up}}^h]$  is the result of interval HSE at time  $k$ ;  $\hat{\mathbf{x}}_{k,\text{up}}^h$  and  $\hat{\mathbf{x}}_{k,\text{down}}^h$  are the upper and lower bounds of the interval HSE value at time  $k$ , respectively;  $x_i^h$  is the actual state value of bus  $i$ ;  $\hat{x}_i^h$  is the interval HSE value of bus  $i$ ;  $\mathbf{x}_{k,\text{up}}^h$  and  $\mathbf{x}_{k,\text{down}}^h$  are the upper and lower bounds of the interval state calculated by MC respectively;  $N$  is the number of states; and  $\kappa_k$  indicates whether the actual value is in the interval HSE value.

## V. SIMULATION EXAMPLE

### A. Simulation Environment Introduction

To verify the effectiveness of the proposed method, the three-phase asymmetric 34-bus is used as the test system. The distribution network operates at a voltage level of 24.9 kV, with a single-phase line reference power of 2.5 MVA. The photovoltaic generation is connected to phase C at bus 22, while wind power is connected to phase B at bus 34, simulating the imbalance introduced into the system [39], [40]. The simulation software is MATLAB 2023b, and the toolbox is MATPOWER and INTLAB V10.2. In addition, the measurement is configured according to the optimization configuration method in [31], as shown in Fig. 4. Following the configuration outlined above, the

required harmonic measurement data is obtained through harmonic flow calculations.

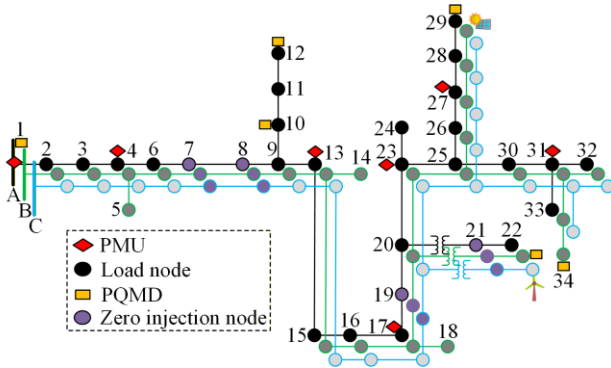


Fig. 4. Improved 34-node distribution network system.

Due to the unavailability of real data, the analysis relies on theoretical models and assumed data. First, the harmonic flow calculation results are used as the true values of the harmonic state, and random errors following a normal distribution are added to these results, which are then used as simulated harmonic measurement values for each harmonic measurement device. The harmonic measurement error of each device is set according to the calibration accuracy of the respective equipment. Different levels of standard deviations are assigned to the measurements and network parameters to simulate their respective uncertainties.

1) For  $\mu$ PMU measurement data, the standard upper and lower limits for current measurement are 0.01% relative to the measured value, and the standard upper and lower limits for voltage measurement are 0.02% relative to the measured value.

2) For PQMD measurement data, the standard upper and lower limits of voltage and current amplitude measurements are 1% of the corresponding measurement values.

Considering the influence of factors such as environmental temperature and line aging on the line parameters, the resistance and reactance values of all lines can be set as  $[0.97rr, 1.03rr]$  and  $[0.98xx, 1.02xx]$  respectively, where  $rr$  and  $xx$  are the rated values of resistance and reactance respectively.

To simulate the asynchrony between measurement devices, it is assumed that the  $\Delta T$  of each PQMD measurement point obeys a normal distribution with a mean of  $0.95T$  and a variance of  $(0.05T)^2$ .

Since PQMD conducts harmonic analysis calculations every 10 cycles and each 3 minutes statistical values are calculated, the sampled series of each PQMD within 24 hours are taken, and a sliding time window of 9 minutes is set. Using the SWWDTW method, the minimum time distance sequence set between the sampled

data of PQMD measurement points and benchmark PQMD measurement points can be obtained. Taking one PQMD series data and benchmark data within a specific time window as the example, the time distance in the time window is shown in Fig. 5, from which it can be seen that the time delay is  $18 \times 10^{-8}$  hours. Based on the time distance alignment data of each point in the time series, the PQMD sequence set with the minimum time distance is obtained, as shown in Fig. 6.

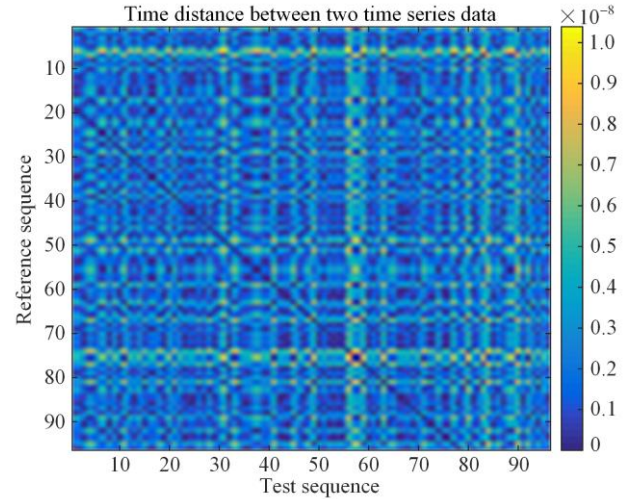


Fig. 5. Time distance between PQMD series and reference series.

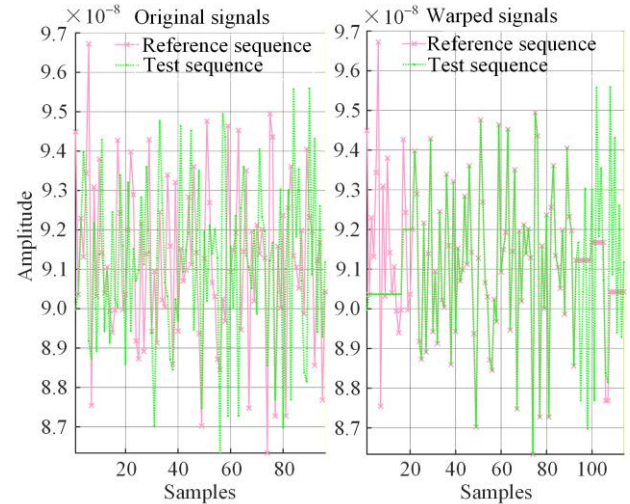


Fig. 6. Alignment time asynchronous sequence.

### B. Effectiveness Analysis of HSE

To evaluate the effectiveness of the proposed harmonic source tracking method, the KMWLS algorithm and the WLS method are used to estimate and decompose the harmonic state. Figure 7 illustrates the interval estimation of phase A node current. Given the high variability in distributed renewable energy output within real distribution networks, obtaining true deterministic state estimation values for comparison is

impractical. Consequently, the interval HSE results derived from the MC method (900 samples per buffer) are used as the reference true value.

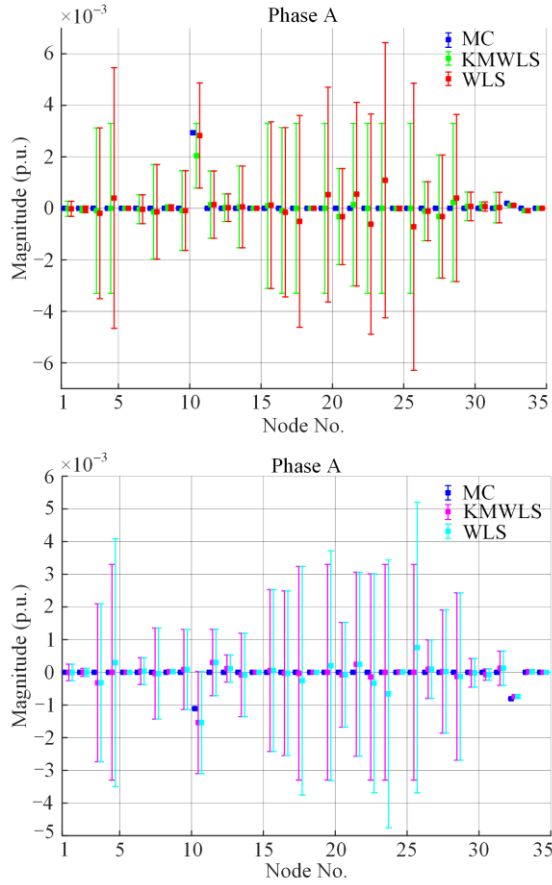


Fig. 7. The interval estimation of phase A node current in the IEEE34-node distribution system.

Taking the real part of phase A in Fig. 7 as an example, the results of KMWLS and WLS calculation can encapsulate the results of MC, which meets the requirements of completeness. From Fig. 7, the interval width of KMWLS is narrower, indicating that the KM operator reduces the interval expansion to a certain extent. The specific performance indicators are shown in Table II. The upper bound of KMWLS interval estimation, root mean square  $\varrho$ , and average conservatism index  $\xi$  are relatively low. Due to the imbalance of three-phase loads, the performance index is particularly prominent in phase A. Root mean square  $\varrho$  of the real and imaginary parts of the node current are decreased by 25% and 12.5%, respectively, and  $\xi$  are decreased by 48.96% and 25.95%, respectively. These results also indicate that HSE in three-phase asymmetric distribution systems needs to consider the three-phase asymmetric load and other factors and cannot be simplified as a symmetric system.

TABLE II  
COMPARISON OF PERFORMANCE INDICATORS BETWEEN INTERVALS

Index	Phase					
		A	B	C		
$\varrho$ (p.u.)	KMWLS	Re	0.0018	0.0017	0.0014	
		Im	0.0016	0.0015	0.0012	
	WLS	Re	0.0024	0.0018	0.0015	
		Im	0.0018	0.0015	0.0012	
$\zeta$ (%)	KMWLS	Re	100	100	100	
		Im	100	100	100	
	WLS	Re	100	100	100	
		Im	100	100	100	
$\xi$ (p.u.)	KMWLS	Re	0.9101	0.0526	0.0419	
		Im	1.7833	0.0174	0.6768	
	WLS	Re	1.3258	0.5307	0.0423	
		Im	1.7904	0.1753	0.6768	

### C. Impact of Time Asynchronous Measurement Data Set

To further analyze the impact of multi-source measurements on interval HSE results, the time asynchronous measurements with varying degrees are set up. The multi-source data fusion method is used to form asynchronous datasets with different deviations, and the effectiveness of the method is verified.

There are two cases of time asynchrony setting for the installed PQMD measuring device. Taking bus 32 as an example, the results are shown in Table III. It can be seen that the greater the time asynchrony of the measurement, the greater the estimation error. Compared to the estimation results without the fusion strategy, the results with the fusion strategy have smaller errors, indicating the effectiveness of the multi-source measurement fusion in reducing measurement errors caused by measurement bias. However, the multi-source data fusion methods cannot fundamentally eliminate the time asynchronism of measurements, which is the inherent characteristic of the PQMD measuring devices.

TABLE III  
HSE RESULTS UNDER DIFFERENT MEASUREMENT DEVIATIONS

PQMD asynchronous time error	Case of time asynchrony setting			
	$0.9T \pm (0.1T)^2$		$0.8T \pm (0.2T)^2$	
Whether to use a multi-source fusion strategy	No	Yes	No	Yes
Relative error of amplitude lower bound (%)	20.8648	8.2202	39.1568	22.9312
Relative error of amplitude upper bound (%)	15.8187	5.7654	45.8121	23.5650
Relative error of lower bound of phase angle (%)	5.6013	4.3935	26.4465	19.5260
Relative error of phase angle upper bound (%)	23.3566	6.6420	26.5541	22.8098

### D. Influence of Measurement Errors

The maximum permissible error for harmonic measurement is less than 5% of the measured value [41]. Accordingly, this paper applies different measurement errors to verify the effectiveness of the proposed method. Figures 8 and 9 show the performance

evaluation indicators of HSE under different measurement errors. When the network parameter deviation remains unchanged (the line parameter deviation range is set to 2%), the proposed method shows a small increase as the measurement error increases.

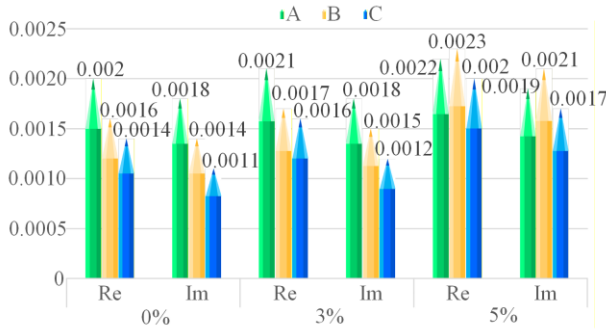


Fig. 8. Estimated upper bound root-mean-square performance index results considering different measurement errors.

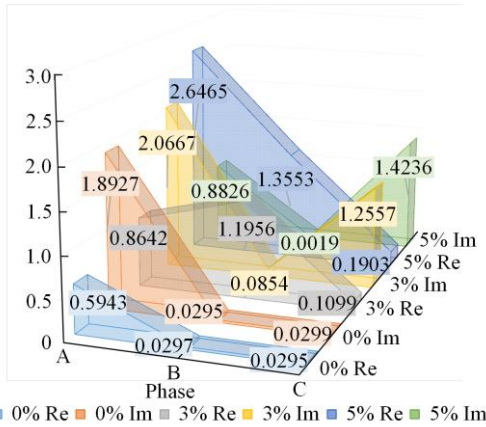


Fig. 9. Average conservative performance index results considering different measurement errors.

Taking phase A as an example, the real and imaginary parts of  $\vartheta$  are increased by up to 5% and 5.56%, respectively; while the real and imaginary parts of  $\xi$  are increased by up to 345.31% and 9.19%, respectively. Since the proposed method uses intervals as model inputs, larger measurement errors lead to wider interval measurements. Consequently, the average conservatism of the interval HSE is doubled. This shows that for interval measurement data, the greater measurement errors, the greater the influence on the interval estimation results.

E. Uncertainty Analysis of Line Parameters

To further analyze the impact of line parameter uncertainty on interval HSE results, this paper assigns different levels of uncertainties to the line resistance and reactance values, thereby expanding the fluctuation range of line parameters. Figures 10 and 11 show the performance evaluation indicators of HSE considering line parameter changes. When the measurement error remains unchanged (the measurement deviation range is set to 1%), each indicator increases to a certain extent as the network parameter deviation increases.

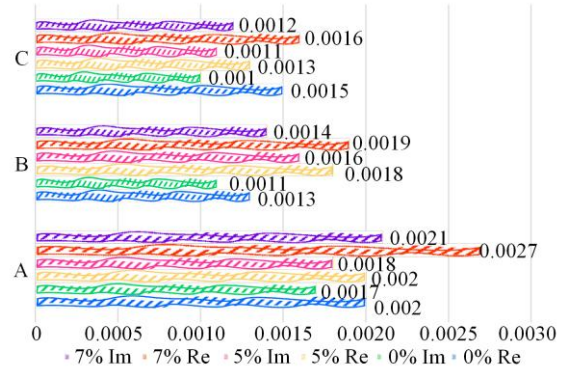


Fig. 10. Estimated upper bound root-mean-square performance index results considering line parameter variation.

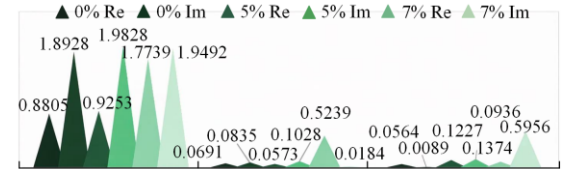


Fig. 11. Average conservative performance index results considering line parameter variation.

Taking phase A as an example, the real and imaginary parts of  $\vartheta$  are increased by up to 14% and 23.53%, respectively; while the real and imaginary parts of  $\xi$  are increased by up to 101.47% and 4.75%, respectively. It can be seen that the deviation of network parameters has a certain impact on the HSE. Because the deviation of network parameters changes the mapping relationship between the harmonic source distribution vector and state sufficient statistics to a certain extent, the trained model cannot represent the actual mapping relationship, and the accuracy of the model decreases.

F. Effectiveness of Harmonic Source Traceability

The harmonic source location based on HSE operates on the following principle. Assuming the estimated value of the  $h$ th injected harmonic current exceeds the maximum allowable value for that node, in this case, it is determined to be an  $h$ th harmonic source. The estimated amplitude of the harmonic state of each bus under the 5th, 7th, and 11th harmonics is identified. The results are shown in Figs. 12–14. As seen, KMWLS can precisely identify harmonic sources at phase A of 10 buses and bus 32, indicating the effectiveness of the proposed HSE method.

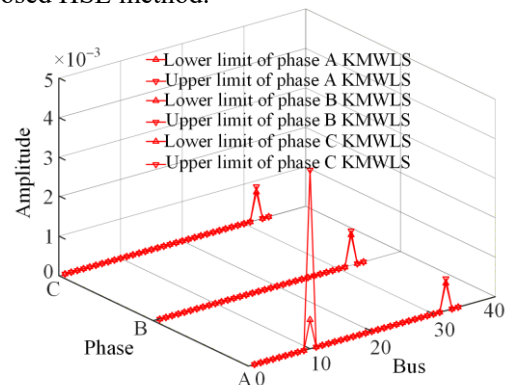


Fig. 12. Results of locating the 5th harmonic source.

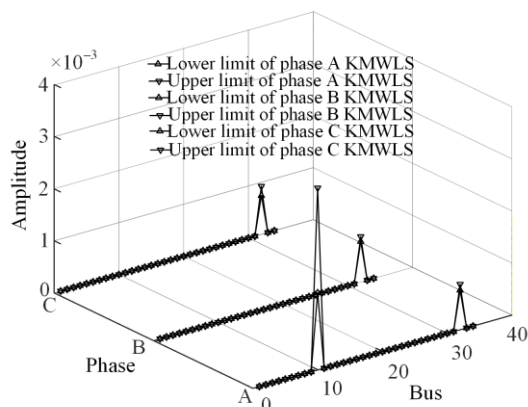


Fig. 13. Results of locating the 7th harmonic source.

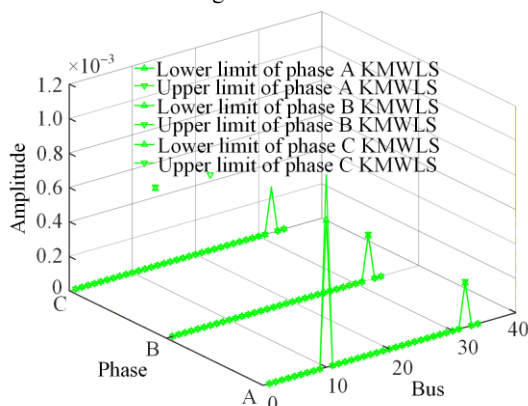


Fig. 14. Results of locating the 11th harmonic source.

**G. Robustness Tests**

To validate the robustness of the proposed method, experiments are conducted within the 123-bus network. The network structure is shown in Fig. 15, with the installation nodes of measurement devices detailed in Table IV. The measurement error setting of each measuring device is the same as that of the 34-bus network. Measurement devices are installed at 21.6% of the total network nodes, a proportion consistent with the sparse distribution of real distribution networks and reflecting the limitations of measurement device deployment in actual distribution networks. The analysis is carried out in this environment to prove the adaptability of the proposed method in practical application.

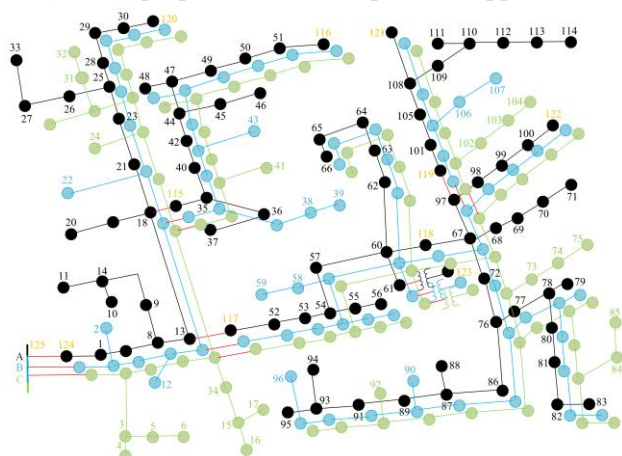


Fig. 15. IEEE123 three-phase network.

TABLE IV  
MEASUREMENT LOCATION IN TEST SYSTEMS

Measurement types	Placement locations
$\mu$ PMU	13, 25, 35, 54, 60, 67, 108, 125
PQMD	3, 15, 21, 44, 47, 51, 64, 70, 74, 78, 81, 86, 93, 99, 101, 103, 110, 122, 123

To verify the effectiveness of the multi-source measurement fusion method, simulations are conducted in the aforementioned environment, using phase A as an example. The 5th harmonic results are shown in Fig. 16. It can be seen that the WLS method using a single type of measurement device leads to misjudgments in harmonic source localization. In contrast, the multi-source measurement fusion technique improves the system’s observability, and the KMWLS method effectively locates harmonic sources.

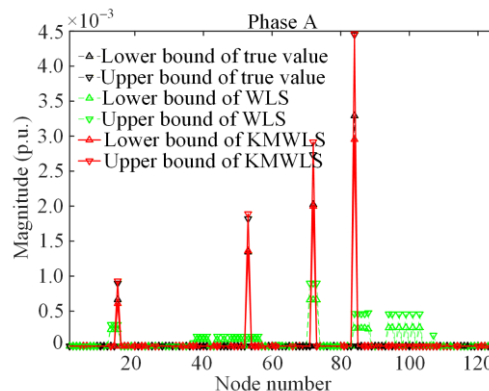


Fig. 16. The estimated amplitude of each node.

Subsequently, based on multi-source measurement fusion, the original KM algorithm is introduced for comparison, using phase C as an example. The specific results are shown in Fig. 17. It can be observed that the KMWLS algorithm offers finer interval widths, enabling more accurate harmonic state estimation results.

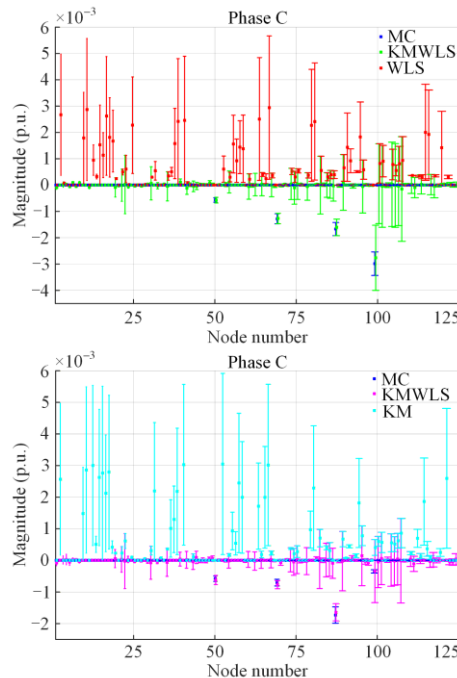


Fig. 17. Real and imaginary parts of phase C node current.

## VI. CONCLUSION

This paper proposes a multi-source asynchronous harmonic data fusion strategy for distribution networks, which avoids incompatibilities between multi-source data and improves the observability of harmonic state estimation. Meanwhile, a three-phase asymmetric harmonic state estimation model is established, and the interval method is used to reflect the uncertainty of the harmonic operation status in the three-phase distribution network. The proposed method is validated on the IEEE-34 and IEEE-123 systems. The results show that the proposed method can be applied to distribution networks with limited harmonic measurement devices, and is capable of harmonic source localization. Future research can focus on developing dynamic harmonic state estimation methods that account for the harmonic characteristics of distributed renewable energy sources.

### ACKNOWLEDGMENT

Not applicable.

### AUTHORS' CONTRIBUTIONS

Lipeng Zhou: overall design and thesis writing of the research. Zhenguo Shao: rigorous analysis and framework construction of the experiment. Guoyang Cheng: data analysis and writing guidance. Junjie Lin: literature review and theoretical support. Feixiong Chen: revision of the paper and the language polishing. All authors read and approved the final manuscript.

### FUNDING

This work is supported by the National Natural Science Foundation of China (No. 52377087).

### AVAILABILITY OF DATA AND MATERIALS

Please contact the corresponding author for data material requests.

### DECLARATIONS

Competing interests: The authors declare that they have no known competing financial interests or personal relationships that could have appeared to influence the work reported in this paper.

### AUTHORS' INFORMATION

**Lipeng Zhou** received the M.S. degree in electrical engineering from the College of Electrical Engineering and New Energy, China Three Gorges University, Yichang, China, in 2022. He is currently studying for a Ph.D. in the College of Electrical Engineering and Automation of Fuzhou University. His main research interests include artificial intelligence techniques in automatic generation control and harmonic state estimation of power systems.

**Zhenguo Shao** received the B.S., M.S., and Ph.D. degrees in electrical engineering from Southeast University, Nanjing, China, in 1992, 2001, and 2004, respectively. From 1992 to 1995, he was an electrical engineer with the Nantong Hong Yang Industrial Company Ltd. From 1995 to 1998, he was a lecturer at Nantong University. From 2004 to 2006, he was a postdoctoral researcher with the Fujian Electric Power Company. Since 2006, he has been with the College of Electrical Engineering and Automation, Fuzhou University, Fuzhou, China, where he is a full professor and dean. He is also the director of the Fujian Smart Electrical Engineering Technology Research Center. His main research interests include power quality monitoring and mitigation, smart grid control and operation, smart energy utilization, and big data analysis for smart grid.

**Guoyang Cheng** received the B.Eng. degree in information systems from the National University of Defense Technology, Changsha, China, in 1992, the M.Eng. degree in control engineering from Tsinghua University, Beijing, China, in 1995, and the Ph.D. degree from the National University of Singapore (NUS), Singapore, in 2006. Since 2006, he has been with the College of Electrical Engineering and Automation, Fuzhou University, Fuzhou, China, where he is now a professor. His research interests include motion control and mechatronics systems.

**Junjie Lin** received the B.S. and Ph.D. in electrical engineering from Tsinghua University, Beijing, China, in 2020 and 2015, respectively. He is currently an associate professor with the College of Electric Engineering and Automation, Fuzhou University, Fuzhou, China. His main research interests include power system operation and stability, synchronous phasor measurement technologies.

**Feixiong Chen** received the B.S. degree in electrical engineering from the Chongqing University of Technology, in 2012, and the Ph.D. degree in electrical engineering from Chongqing University, Chongqing, China, in 2017. From 2016 to 2017, he was a visiting Ph.D. student with the Department of Electrical and Computer Engineering, Wayne State University, Detroit, MI, USA. From 2017 to 2018, he was a research associate with the Department of Electrical Engineering, The Hong Kong Polytechnic University, Hong Kong, China. Since 2019, he has been with the Fujian Smart Electrical Engineering Technology Research Center, College of Electrical Engineering and Automation, Fuzhou University, Fuzhou, China. His current research interests include distributed control and optimization methods of energy internet and energy trading in distribution networks.

## REFERENCES

- [1] G. Cheng, Y. Lin, and A. Abur *et al.*, "A survey of power system state estimation using multiple data sources: PMUs, SCADA, AMI, and beyond," *IEEE Transactions on Smart Grid*, vol. 15, no. 1, pp. 1129-1151, Jan. 2024.
- [2] X. Xie, J. Zhang, and Y. Sun *et al.*, "A measurement-based dynamic harmonic model for single-phase diode bridge rectifier-type devices," *IEEE Transactions on Instrumentation and Measurement*, vol. 73, no. 1501111, pp. 1-13, Feb. 2024.
- [3] Z. Dai and W. Lin, "Adaptive estimation of three-phase grid voltage parameters under unbalanced faults and harmonic disturbances," *IEEE Transactions on Power Electronics*, vol. 32, no. 7, pp. 5613-5627, Jul. 2017.
- [4] J. Yu, D. Yang, and J. Cao *et al.*, "Robust state estimation for an electricity-gas-heat integrated energy system considering dynamic characteristics," *Protection and Control of Modern Power Systems*, vol. 9, no. 1, pp. 65-80, Jan. 2024.
- [5] L. Cristaldi and A. Ferrero, "Harmonic power flow analysis for the measurement of the electric power quality," *IEEE Transactions on Instrumentation and Measurement*, vol. 44, no. 3, pp. 683-685, Jun. 1995.
- [6] F. Xu, H. Yang, and J. Zhao *et al.*, "Study on constraints for harmonic source determination using active power direction," *IEEE Transactions on Power Delivery*, vol. 33, no. 6, pp. 2683-2692, Dec. 2018.
- [7] L. Ji, J. Yin, and E. Jiang *et al.*, "A fault location method based on hybrid measurement state estimation for a distribution network," *Power System Protection and Control*, vol. 52, no. 12, pp. 58-68, Jun. 2024. (in Chinese)
- [8] J. Zhang, T. Bi, and H. Liu, "A comprehensive evaluation and analysis system for accuracy of power system state estimation," *Power System Protection and Control*, vol. 52, no. 20, pp. 12-24, Oct. 2024. (in Chinese)
- [9] A. L. Langner and A. Abur, "Formulation of three-phase state estimation problem using a virtual reference," *IEEE Transactions on Power Systems*, vol. 36, no. 1, pp. 214-223, Jan. 2021.
- [10] W. Zheng, W. Huang, and D. J. Hill *et al.*, "An adaptive distributionally robust model for three-phase distribution network reconfiguration," *IEEE Transactions on Smart Grid*, vol. 12, no. 2, pp. 1224-1237, Mar. 2021.
- [11] S. Song, X. Hao, and Y. Lin *et al.*, "Robust three-phase state estimation for PV-integrated unbalanced distribution systems," *Applied Energy*, vol. 322, pp.1-15, Sep. 2022.
- [12] T. D. Kahingala, S. Perera, and U. Jayatunga *et al.*, "Estimation of voltage unbalance attenuation caused by three-phase induction motors: an extension to distribution system state estimation," *IEEE Transactions on Power Delivery*, vol. 34, no. 5, pp. 1853-1864, Oct. 2019.
- [13] B. Zargar, A. Angioni, and F. Ponci *et al.*, "Multiarea parallel data-driven three-phase distribution system state estimation using synchrophasor measurements," *IEEE Transactions on Instrumentation and Measurement*, vol. 69, no. 9, pp. 6186-6202, Sep. 2020.
- [14] Z. Cao, Y. Wang, and C. Chu *et al.*, "Robust pseudo-measurement modeling for three-phase distribution systems state estimation," *Electric Power Systems Research*, vol. 180, pp. 1-10, Mar. 2020.
- [15] D. Xu, Z. Wu, and J. Xu *et al.*, "A multiarea forecasting-aided state estimation strategy for unbalance distribution networks," *IEEE Transactions on Industrial Informatics*, vol. 20, no. 1, pp. 806-814, Jan. 2024.
- [16] Y. Wang, Y. Li, and Y. Liu *et al.*, "Optimal placement method for monitoring devices under unknown harmonic source information in distribution networks," *Power System Protection and Control*, vol. 53, no. 19, pp. 162-174, Oct. 2025. (in Chinese)
- [17] A. Akrami, S. Asif, and H. Mohsenian-Rad, "Sparse tracking state estimation for low-observable power distribution systems using D-PMUs," *IEEE Transactions on Power Systems*, vol. 37, no. 1, pp. 551-564, Jan. 2022.
- [18] T. Liu, Q. Shu, and F. Xu *et al.*, "A method for determining harmonic contribution and harmonic source current based on minimum mutual information and bayesian optimization," *IEEE Transactions on Instrumentation and Measurement*, vol. 73, pp. 1-8, Sep. 2024.
- [19] F. Ahmadi-Gorjaji and H. Mohsenian-Rad, "A physics-aware MIQP approach to harmonic state estimation in low-observable power distribution systems using harmonic phasor measurement units," *IEEE Transactions on Smart Grid*, vol. 14, no. 3, pp. 2111-2124, May 2023.
- [20] F. Xu, C. Wang, and K. Guo *et al.*, "Harmonic sources' location and emission estimation in underdetermined measurement system," *IEEE Transactions on Instrumentation and Measurement*, vol. 70, no. 9003511, pp. 1-11, May 2021.
- [21] J. Zhang, Y. Wang, and Y. Weng *et al.*, "Topology identification and line parameter estimation for non-PMU distribution network: a numerical method," *IEEE Transactions on Smart Grid*, vol. 11, no. 5, pp. 4440-4453, Sep. 2020.
- [22] V. H. P. d. Melo, J. A. D. Massignan, and J. B. A. London, "Angular reference problem for three-phase distribution system state estimation," *IEEE Transactions on Power Systems*, vol. 39, no. 3, pp. 5138-5149, May 2024.
- [23] Z. Liu, P. Li, and C. Wang *et al.*, "Robust state estimation of active distribution networks with multi-source measurements," *Journal of Modern Power Systems and Clean Energy*, vol. 11, no. 5, pp. 1540-1552, Sep. 2023.
- [24] D. Xu, J. Xu, and C. Qian *et al.*, "A pseudo-measurement modelling strategy for active distribution networks considering uncertainty of DGs," *Protection and Control of Modern Power Systems*, vol. 9, no. 5, pp. 1-15, Sep. 2024.
- [25] M. Kabiri and N. Amjadi, "A new hybrid state estimation considering different accuracy levels of PMU and SCADA measurements," *IEEE Transactions on Instrumentation and Measurement*, vol. 68, no. 9, pp. 3078-3089, Sep. 2019.
- [26] A. S. Dobakhshari, M. Abdolmaleki, and V. Terzija *et al.*, "Robust hybrid linear state estimator utilizing SCADA and PMU measurements," *IEEE Transactions on Power Systems*, vol. 36, no. 2, pp. 1264-1273, Mar. 2021.

- [27] S. Li, Y. He, and H. Wu *et al.*, "Dynamic state estimation for distribution networks based on adaptive set membership filter under unknown but bounded noise environments," *IEEE Sensors Journal*, vol. 24, no. 8, pp. 12654-12666, Apr. 2024.
- [28] W. Zhou, O. Ardakanian, and H. Zhang *et al.*, "Bayesian learning-based harmonic state estimation in distribution systems with smart meter and DPMU data," *IEEE Transactions on Smart Grid*, vol. 11, no. 1, pp. 832-845, Jan. 2020.
- [29] Y. Wang, H. Ma, and X. Xiao *et al.*, "Harmonic state estimation for distribution networks based on multi-measurement data," *IEEE Transactions on Power Delivery*, vol. 38, no. 4, pp. 2311-2325, Aug. 2023.
- [30] X. Chen, C. Yang, and Y. Zhang *et al.*, "Multi-source data driven harmonic spectrum estimation of substation feeder current," *Energy Reports*, vol. 11, pp. 3492-3500, Jun. 2024.
- [31] Q. Shu, H. Wang, and C. Wang *et al.*, "A multiharmonic sources localization algorithm based on ICA and posterior harmonic admittance," *IEEE Transactions on Instrumentation and Measurement*, vol. 73, pp. 1-10, Dec. 2024.
- [32] I. D. Melo and M. P. Antunes. "Bad data correction in harmonic state estimation for power distribution systems: an approach based on generalized pattern search algorithm," *Electric Power Systems Research*, vol. 204, pp. 1-11, Mar. 2022.
- [33] J. Enayati, A. Rahimnejad, and L. Vanfretti *et al.*, "Dynamic harmonic estimation using a novel robust filtering strategy: iterated sliding innovation cubature Filter," *IEEE Transactions on Instrumentation and Measurement*, vol. 72, pp. 1-10, Nov. 2023.
- [34] I. D. Melo, J. L. R. Pereira, and P. F. Ribeiro *et al.*, "Harmonic state estimation for distribution systems based on optimization models considering daily load profiles," *Electric Power Systems Research*, vol. 170, pp. 303-316, May 2019.
- [35] Y. Chen, Z. Shao, and Y. Zhang, "Distribution network parameter estimation method based on interval harmonic state estimation and prediction-correction," in *2023 8th Asia Conference on Power and Electrical Engineering (ACPEE)*, Tianjin, China, Apr. 2023, pp. 32-37.
- [36] C. Rakpenthai, S. Uatrongjit, and N. R. Watson *et al.*, "On harmonic state estimation of power system with uncertain network parameters," *IEEE Transactions on Power Systems*, vol. 28, no. 4, pp. 4829-4838, Nov. 2013.
- [37] S. Salvador and P. Chan, "Toward accurate dynamic time warping in linear time and space," *Intelligent Data Analysis*, vol. 11, no. 5, pp. 561-580, Jan. 2007.
- [38] M. Neshat, G. Sepidnam, and M. Sargolzaei *et al.*, "Artificial fish swarm algorithm: a survey of the state-of-the-art, hybridization, combinatorial and indicative applications," *Artificial intelligence review*, vol. 42, no. 4, pp. 965-997, Dec. 2014.
- [39] L. Wu, Y. Wang, and Y. Wang *et al.*, "Cellular computational networks based hierarchical data-driven dynamic state estimation method considering uncertainties," *Protection and Control of Modern Power Systems*, vol. 10, no. 2, pp. 150-161, Mar. 2025.
- [40] C. Zhang, Z. Shao, and C. Jiang *et al.*, "A PV generation data reconstruction method based on improved super-resolution generative adversarial network," *International Journal of Electrical Power & Energy Systems*, vol. 132, pp. 1-12, Nov. 2021.
- [41] Electromagnetic Compatibility (EMC)-Part 4-7: Testing and Measurement Techniques-General Guide on Harmonics and Interharmonics Measurements and Instrumentation for Power Supply Systems and Equipment Connected Thereto, IEC Standard 61000-4-7, 2008.